Eur. Phys. J. E **24**, 367–377 (2007)
DOI 10.1140/epje/i2007-10247-7

THE EUROPEAN PHYSICAL JOURNAL E

Brownian particles in random and quasicrystalline potentials: How they approach the equilibrium

M. Schmiedeberg[1,a], J. Roth[2], and H. Stark[1]

[1] Institut für Theoretische Physik, Technische Universität Berlin, Hardenbergstr. 36, D-10623 Berlin, Germany
[2] Institut für Theoretische und Angewandte Physik, Universität Stuttgart, Pfaffenwaldring 57, D-70550 Stuttgart, Germany

Received 13 August 2007 and Received in final form 30 October 2007
Published online: 18 January 2008 –

Abstract. We study the Brownian motion of an ensemble of single colloidal particles in a random square and a quasicrystalline potential when they start from non-equlibrium. For both potentials, Brownian dynamics simulations reveal a widespread subdiffusive regime before the diffusive long-time limit is reached in thermal equilibrium. We develop a random trap model based on a distribution for the depths of trapping sites that reproduces the results of the simulations in detail. Especially, it gives analytic formulas for the long-time diffusion constant and the relaxation time into the diffusive regime. Aside from detailed differences, our work demonstrates that quasicrystalline potentials can be used to mimic aspects of random potentials.

PACS. 82.70.Dd Colloids – 05.40.Jc Brownian motion – 61.44.Br Quasicrystals

1 Introduction

Free Brownian motion that leads to diffusion at time scales where inertia can be neglected is well understood since Einstein's seminal paper [1]. It serves as a paradigm for soft matter and biological physics [2]. In recent years more and more systems have been studied that due to confinement or external potentials are subdiffusive, *i.e.*, the mean-square displacement of the random walker does not increase linearly in time but behaves as $\langle r^2 \rangle \propto t^\nu$ with an exponent $\nu < 1$. Examples are many-particle systems, such as dense colloidal suspensions close to freezing [3], or other glassy systems (see, *e.g.*, [4,5]), where subdiffusion is due to caging from surrounding particles, as demonstrated explicitely in experiments [6]. Permanent confinement leads to subdiffusion as well: particles that move in narrow channels exhibit anomalous diffusion [7] which recently was also studied for colloidal systems [8–10]. Furthermore, particles confined to the fractal space between obstacles forming a Lorentz gas behave subdiffusively on intermediate time scales [11]. Anomalous diffusion also plays an important role in many biological systems. Examples are the dynamics of molecular motors moving along heterogeneous substrates [12], the subdiffusion of macromolecules in the cell due to crowding [13], the motion of beats in the cytoskeleton or artificial actin networks [14,15], or the dynamics of flurescently labeled molecules in cells [16–18] and in membranes [19]. However, even the simple Brownian motion of a single particle in a random potential exhibits subdiffusion. Honkonen and Pis'mak [20] showed that such a motion is subdiffusive on all time scales if the depth of the potential is not limited from below. This was extensively studied in many Brownian dynamics simulations [21–23]. Yet, as soon as each potential well possesses a finite depth, the motion always becomes diffusive in the long-time limit. Modeling it by jumps between traps with random but finite strengths, the diffusion constant can be calculated (see, *e.g.*, Haus *et al.* in [24,25] or Derrida in [26]).

Normally, diffusion is studied in thermal equilibrium. Here we investigate how Brownian particles reach the diffusive long-time limit via a subdiffusional regime when they start from non-equilibrium. Especially, we will compare Brownian motion in three types of two-dimensional potential landscapes, namely a regular and a random square lattice and a potential with quasicrystalline symmetry (see Fig. 1). We will show that, although the quasicrystalline potential possesses long-range order, it behaves similar to a random potential. Since their discovery [27] quasicrystals have conveyed much fascination, mainly because our understanding of what crystals are had to change substantially [28]. Transport processes in quasicrystals depend crucially on the quasicrystalline order (see, *e.g.*, [29]) and have stimulated, *e.g.*, the study of atomic diffusion in optical quasicrystals [30]. On the other hand, there is now an increasing interest in how atoms order and move on quasicrystalline surfaces [31–37]. This was one motivation for us to start the work presented in this article. Although our investigation is purely theoretical, we have in mind colloidal particles in a fluid

[a] e-mail: michael.schmiedeberg@tu-berlin.de

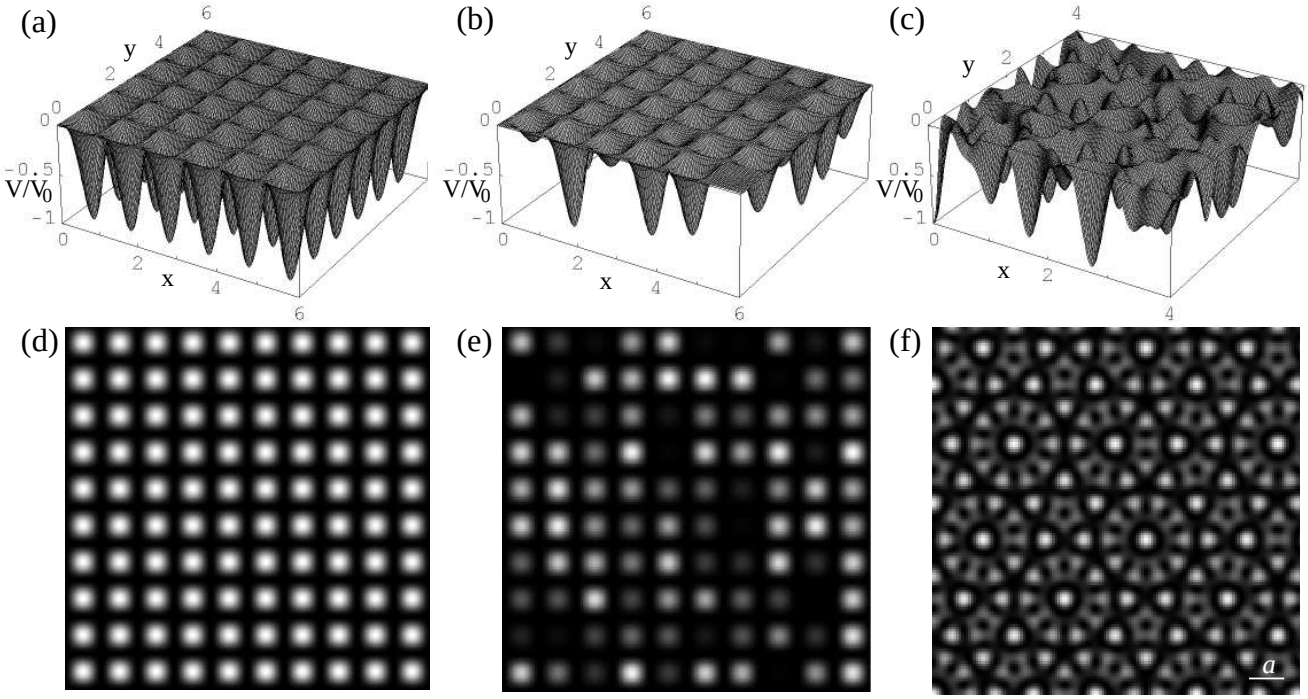

Fig. 1. (a–c) Potential landscapes and (d–f) their grey-scale representations for (a,d) a regular square, (b,e) a random square, and (c,f) a decagonal potential. The exact definitions of the potentials are given in Section 2. The bar in the lower right corner of (f) indicates the characteristic length $a = 2\pi/|\mathbf{G}_j|$.

environment. They are widely used as a model system for statistical mechanics, for atomic systems, and for investigating the non-equilibrium. Especially, they are the ideal choice to study Brownian motion in an external potential. As first demonstrated by Ashkin, colloids can be manipulated by laser fields since they are locally forced towards the highest field strengths [38]. Therefore, intensity patterns from interfering laser beams create new complex colloidal structures also referred to as optical matter [39]. In such a system various phenomena such as crystallization and light-induced ordering or different melting transitions have been studied [40–43].

In this paper, we explore the dynamics of Brownian particles in external potentials, especially the subdiffusion-diffusion transition and its relation to the non-equilibrium. We perform Brownian dynamics simulations in a regular and a random square potential and a potential landscape with quasicrystalline symmetry in order to monitor the mean-square displacement of a single particle and its average potential energy. We then develop a random trap model based on the probability distribution $P(V_m, t)$ for finding a particle at time t in a potential well of depth V_m. The model is able to explain the main features of our Brownian dynamics simulations. It especially clarifies that the transition from subdiffusion to diffusion is due to a relaxation process of the distribution $P(V_m, t)$ into a stationary state, where $P(V_m, t)$ no longer depends on time. The model quantitatively predicts the time scale for this relaxation process and is able to give an estimate for the diffusion constant in the long-time limit. It furthermore reproduces characteristic differences in the temporal evolution of the particle's average potential energy in the random-square and the quasicrystalline potential due to the different distributions of the depths V_m of the potential minima.

The paper is organized as follows. In Section 2 we introduce our model, describe the details of the Brownian dynamics simulations and define the potential landscapes used in this article. The results of the Brownian dynamics simulations are summarized in Section 3 and a first interpretation of our findings is given. In Section 4 the random trap model is developed. Its results, also in comparison to the Brownian dynamics simulations, are presented and discussed in Section 5 before we conclude our work in Section 6.

2 Model

In our theoretical modelling, we consider a single colloidal particle that moves in an external potential in two dimensions only. This could mimic, *e.g.*, the motion of an atom on a quasicrystalline surface.

2.1 Brownian dynamics simulations

To access the dynamics of the colloidal particle in different types of potentials, we perform Brownian dynamics simulations where we solve the overdamped Langevin equation

$$\gamma \frac{\mathrm{d}}{\mathrm{d}t}\mathbf{r} = -\nabla V(\mathbf{r}) + \mathbf{f}(t). \tag{1}$$

Here $\mathbf{r}$ denotes the position of the particle in the xy-plane and γ its friction coeffcient. The external potential $V(\mathbf{r})$ is specified below. The thermal force $\mathbf{f}(t)$ is realized by random kicks with zero mean, $\langle \mathbf{f}(t) \rangle = 0$, and two-point correlations given by the fluctuation-dissipation theorem, $\langle f_i(t) f_j(t') \rangle = 2\gamma k_B T \delta_{ij} \delta(t - t')$. The initial positions of the colloids are chosen randomly and all results presented are averages over 5000 runs. The time steps in the simulations are automatically chosen such that none is longer than $0.005\beta\gamma a^2$ and no step length exceeds $0.02a$. The simulation of a curve in Figure 4 typically takes several weeks on a state-of-the-art computer [44].

In the following, we introduce the external potentials that we use in our simulations.

2.2 Square potentials

We first consider simple regular and random square potentials (see Figs. 1(a) and (b)). They possess minima located on a square grid with a lattice constant a. On each position $\mathbf{r}_m = (x_m, y_m)$ of the minima, a potential well is placed that extends throughout an area given by $|x - x_m| \leq a/2$ and $|y - y_m| \leq a/2$:

$$V(\mathbf{r}) = -\frac{V_m(\mathbf{r}_m)}{2} \times \left\{ 1 + \cos\left[\frac{2\pi(x - x_m)}{a}\right] \cos\left[\frac{2\pi(y - y_m)}{a}\right] \right\}, \quad (2)$$

where $V_m(\mathbf{r}_m)$ is the depth of the minimum at $\mathbf{r}_m$.

In the regular square potential, $V_m(\mathbf{r}_m) = V_0 = \text{const}$ for all minima, *i.e.*, the regular square potential is periodic. For the random square potential, $V_m(\mathbf{r}_m)$ is taken randomly from the intervall $[0, V_0]$ with the same probability for all possible depths.

2.3 Decagonal potential

Five interfering laser beams, as illustrated in Figure 2(a), create a light field, also called optical lattice [39,45]. By construction it possesses a long-range positional order, however, with a non-crystallographic point group symmetry. Such potentials are, therefore, denoted quasiperiodic. In our case, a decagonal potential occurs, *i.e.*, it exhibits a tenfold rotational point symmetry. For vanishing tilt angle $\theta \to 0$ and identical polarization vectors (see Fig. 2(a)), the external potential in the xy-plane ($z = 0$) is [45]

$$V(\mathbf{r}) = -\frac{V_0}{25} \sum_{j=0}^{4} \sum_{k=0}^{4} \cos[(\mathbf{G}_j - \mathbf{G}_k) \cdot \mathbf{r}], \quad (3)$$

where $\mathbf{G}_j$ are the wave vectors of the beams projected onto the xy-plane (see Fig. 2(b)). To arrive at equation (3), one calculates the intensity of the interfering laser beams and then takes the average over one period of the oscillating light field. The prefactor is chosen such that $-V_0$ gives the minimum value of the potential. Figures 1(c) and (f) show, respectively, a three-dimensional and a gray-scale representation of the decagonal potential.

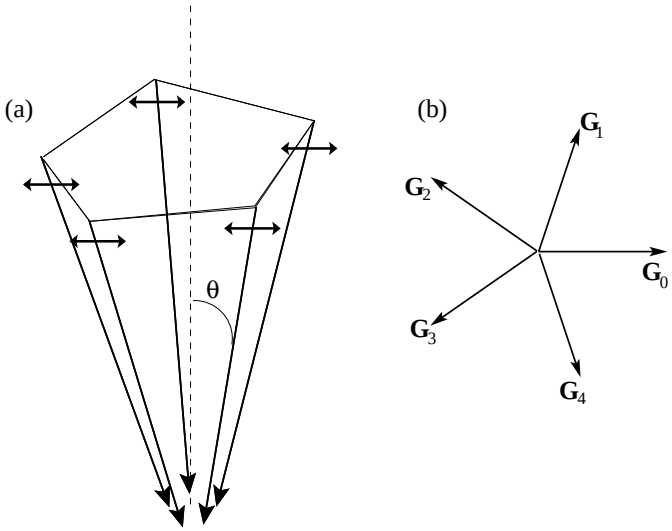

Fig. 2. (a) Five laser beams, whose projections along the vertical line onto the xy-plane form a pentagon, interfere and produce a potential landscape for a colloidal particle. In the following, the angle θ is assumed to be small. Then the polarization vectors of the five laser beams can be chosen the same without distroying the decagonal symmetry in the xy-plane. (b) The five wave vectors of the beams projected onto the xy-plane.

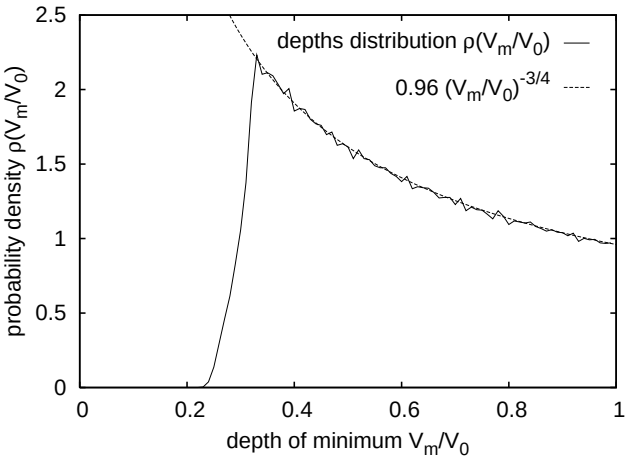

Fig. 3. Probability density $\rho(V_m)$ of the depths of the minima in the decagonal potential. The dashed line behaves as $V_m^{-3/4}$.

In addition, Figure 3 illustrates the probability density $\rho(V_m)$ for the distribution of the depths of the minima in the decagonal potential, *i.e.*, $\rho(V_m)\mathrm{d}V_m$ is the probability for finding a minimum with a depth between V_m and $V_m + \mathrm{d}V_m$. We will employ this probability density in the random trap model of Section 4 and explicitly use it to calculate the mean-square displacement from the model. Figure 3 displays $\rho(V_m)$ as a continuous distribution contrary to the discrete values one would obtain for a periodic potential. The reason is that the decagonal potential (3) is constructed from the superposition of plane waves whose wave vectors are oriented along a pentagon. Therefore,

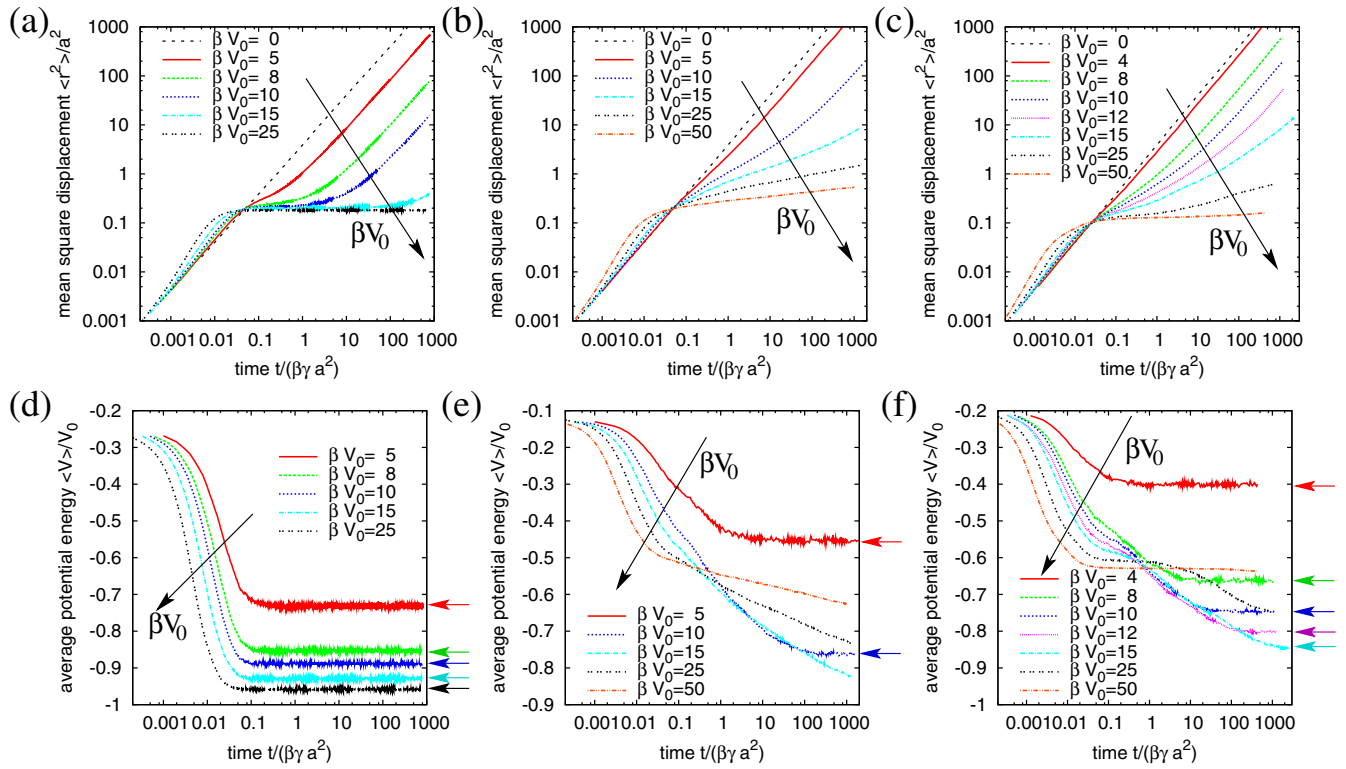

Fig. 4. Results of the Brownian dynamics simulations for the mean-square displacement and the average value of the potential energy of the Brownian particle as a function of time for different types of potentials: (a,d) regular square potential, (b,e) random square potential, (c,f) decagonal potential. The parameter βV_0 increases along the arrows. The small arrows on the right of (d), (e), and (f) indicate that a stationary potential-energy state has been reached. Lengths and times are measured, respectively, in units of a and $\beta\gamma a^2$, where a is the characteristic length scale of the potentials and γ is the particle's friction coefficient.

in any spatial direction one finds a superposition of sinusoidal modulations whose wave numbers are incommensurate to each other. In the literature it is known that in quasicrystalline patterns the distribution of the potential values for minima and maxima can be quite complex [46]. However, in our case we find a rather smooth distribution. Two significant features are visible: minima with depths below $V_m/V_0 < 0.25$ do not exist and, interestingly, we find that for sufficiently large V_m the density $\rho(V_m)$ behaves as $V_m^{-\nu}$ with an exponent $\nu = 3/4$.

We add a last remark. Equation (3) was calculated by assuming the same phase factors for all the five laser beams. Choosing arbitrary phase factors displaces the decagonal potential and also introduces a so-called phasonic shift [47]. We have checked that this does not change our simulation results and the probability density $\rho(V_m)$ just discussed.

3 Results of the simulations

The Brownian dynamics simulations for single particles are performed for the regular square, the random square, and the decagonal potentials introduced in the previous section and illustrated in Figure 1. All of these potentials consist of wells whose depths are limited, therefore we expect normal diffusion for long times as explained in references [24,25]. Here we are also interested in the behavior at short and intermediate time scales of an ensemble of Brownian particles whose starting positions are chosen randomly in space so that the ensemble is not in thermal equilibrium. The upper part of Figure 4 illustrates the mean-square displacement as a function of time for the three types of potential landscapes and for different potential strengths βV_0, where $\beta = 1/(k_B T)$ is the inverse thermal energy. Without potential ($\beta V_0 = 0$), as expected, normal diffusion occurs with $\langle \mathbf{r}^2 \rangle = 4Dt$, where the Einstein relation $D = (\beta\gamma)^{-1}$ relates the diffusion constant D to the particle's friction coefficient γ. When the potential is switched on, the particles relax into the nearest minimum on a short time scale. The relaxation occurs faster for increasing βV_0, *i.e.*, when the strength of the potential becomes larger. Due to this forced relaxation, the mean-square displacement evolves faster than normal diffusion, as can be readily seen in Figures 4(a), (b), and (c). Interestingly, when the particles reach the nearest minimum, all the curves of the mean-square displacement for different potential strengths seem to intersect in a single point. We were not able to explain this feature by a simple argument. In the long-time limit, we find normal diffusion with a diffusion constant that decreases with increasing strength βV_0. At intermediate times, the mean-square displacement

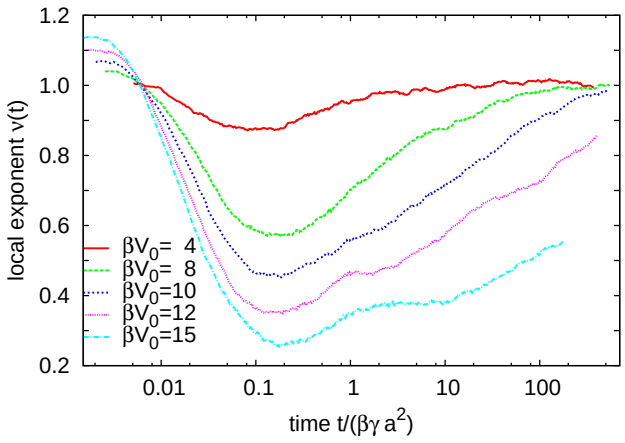

Fig. 5. Time dependence of the local exponent $\nu(t)$ as defined in equation (4) for the decagonal potential.

in the regular square potential does almost not increase and at a value of a^2, where a is the lattice constant, it has already reached the diffusive regime. This means, at the time scale where the particle is able to leave the potential well and makes steps of length a, diffusion sets in immediately. By contrast, in the random square and the decagonal potential, we find a subdiffusional regime which extends over several characterictic lengths a. So here the particles have to explore the potential landscape beyond the local minimum before they can enter normal diffusion. The temporal range of this intermediate regime increases with increasing potential strength βV_0 since it becomes harder for the particles to leave a local minimum by thermal excitation. For high values of V_0, the diffusive regime has not even been reached at the end of the simulation.

Subdiffusion is often characterized by a single exponent ν in the power law for the mean-square displacement $\langle r^2 \rangle \propto t^\nu$. However, in our case subdiffusion cannot be described by such a single power law. We, therefore, plot in Figure 5 the time dependence of

$$\nu(t) = \mathrm{d}\log[\langle r^2(t)\rangle/a^2]/\mathrm{d}\log[t/(\beta\gamma a^2)], \qquad (4)$$

which corresponds to a "local" exponent. As expected, the exponent is larger than 1 for very small times which characterizes superdiffusive motion during the time when the particle relaxes into the nearest minimum from its starting position. For intermediate times, *i.e.*, in the subdiffusive regime ν is smaller than one and relaxes slowly towards the asymptotic diffusive limit where it assumes $\nu = 1$.

To gain further insight, we plot in the lower part of Figure 4 the average potential energy

$$\langle V(t)\rangle = \sum_i^N V(\mathbf{r}_i(t)) \qquad (5)$$

of the ensemble of N particles with position vector $\mathbf{r}_i(t)$ as a function of time t. At the beginning, each particle starts at a random position so the average potential energy of the ensemble is just the mean value of the potential, *i.e.*, $-0.25V_0$ for the regular, $-0.125V_0$ for the random square and $-0.2V_0$ for the decagonal potential. As already explained, at small times the particle relaxes into the closest potential minimum. In the regular square potential, the resulting average potential energy then corresponds to the long-time limit, which is just the canonical ensemble average of the particle's potential energy in a single potential well. In the random square and the decagonal potential, the mean potential energy decreases with time in the subdiffusional regime, *i.e.*, the particles use this regime to explore the landscape for deeper potential wells. Finally, in the long-time limit the constant value of thermal equilibrium (indicated by small arrows in Figs. 4(d), (e), and (f)) is reached at the time when the subdiffusion-diffusion crossover takes place. Again, for high βV_0 this limit is not reached within the simulation time since the average potential energy has not reached the plateau, *i.e.*, its thermal-equilibrium value. Although random square and decagonal potential show the same qualitative behavior, there is also a pronounced difference. In the decagonal potential (see Fig. 4(f)), a plateau of the average potential energy develops with increasing βV_0 on intermediate time scales. The plateau is roughly situated at the average value of V_m and occurs since the particles after the initial fast relaxation into a nearby minimum need time to leave this minimum. However, in the random-square potential only a clear bend develops in the average potential energy when the particles have relaxed in the nearby minima (see Fig. 4(e)). The different behavior is due to the different distributions $\varrho(V_m)$ of the depths of the minima. For the random square potential all V_m occur with the same probability between 0 and V_0. So the particles, when time proceeds, can first leave the shallow minima and populate deeper potential wells which results in a steady decrease of the average potential energy. For the decagonal potential this procedure is hindered by the fact that minima with depths smaller than $0.24V_0$ do not exist (see Fig. 3). Furthermore, $\varrho(V_m)$ decreases with increasing V_m so the probability that Brownian particles find deeper minima also decreases. We will further discuss these differences in Section 5.

4 Random trap model

We now introduce a model that is able to catch the main features of our simulations. In general, the mean-square displacement of a random walker can be calculated by considering its jumps between trapping sites. Here, we assume the local minima of the external potential to be the traps of the colloidal particle. The probability for a jump from one minima to a neighboring one is given by a transition rate Γ. We first assume that it depends quite generally on the location of the respective trapping site. The mean-square displacement of the random walker is calculated by

$$\langle r^2(t)\rangle = \sum_j p(x_j, y_j, t)(x_j^2 + y_j^2), \qquad (6)$$

where $p(x, y, t)$ denotes the probability to be at (x, y) at time t and the sum is over all positions of potential

minima. For the moment, we consider square and also triangular or hexagonal lattices because in these lattices the number of nearest neighbours is constant and the distance between nearest neighbors is always the same. In the decagonal potential this is not the case. Nevertheless, after we have developed the model, we will show that its results well approximate the random walk in the decagonal potential when mean values for the numbers of nearest neighbors and their distances are chosen.

The probability $p(x, y, t)$ has to fulfill the rate equation:

$$\frac{\mathrm{d}}{\mathrm{d}t}p(x_j, y_j, t) = -z\Gamma(x_j, y_j)p(x_j, y_j, t) + \sum_{i\in NN_j} \Gamma(x_i, y_i)p(x_i, y_i, t), \quad (7)$$

where the sum is over all nearest neighbors of the minimum j located at x_j, y_j and z is the number of its nearest neighbors. The first term on the right-hand side of equation (7) describes particles leaving the trap site j and the second term belongs to particles reaching site j from neighboring traps. We define the time-dependent diffusion constant $D(t)$ via $D(t) = \frac{\mathrm{d}}{\mathrm{d}t}\langle r^2(t)\rangle/4$ so that it yields the conventional diffusion constant for normal diffusion. Using equation (7) in equation (6) gives

$$D(t) = \frac{1}{4}\sum_j \Big[- z\Gamma(x_j, y_j)p(x_j, y_j, t) + \sum_{i\in NN_j} \Gamma(x_i, y_i)p(x_i, y_i, t)\Big](x_j^2 + y_j^2). \quad (8)$$

The order of summation in the second term can be interchanged

$$\sum_j \sum_{i\in NN_j} \Gamma(x_i, y_i)p(x_i, y_i, t)(x_j^2 + y_j^2) = \sum_i \sum_{j\in NN_i} \Gamma(x_i, y_i)p(x_i, y_i, t)(x_j^2 + y_j^2), \quad (9)$$

so that for the square, triangular and hexagonal lattice the term

$$\sum_{j\in NN_i} (x_j^2 + y_j^2) = zx_i^2 + zy_i^2 + zl^2\,, \quad (10)$$

can immediately be calculated, where l is the jump length (*e.g.*, the lattice constant a in the square lattice). Using equation (10) in (9), equation (8) becomes

$$D(t) = \frac{zl^2}{4}\sum_j \Gamma(x_j, y_j)p(x_j, y_j, t). \quad (11)$$

In the long-time limit, this is equivalent to the asymptotic, time-independent diffusion constant

$$D_\infty = \frac{zl^2}{4}\langle\langle\Gamma\rangle\rangle, \quad (12)$$

given, *e.g.*, in reference [25], where $\langle\langle\cdot\rangle\rangle$ means an average weighted according to the occupation probabilities of the trapping sites. Note that equation (11) is not only valid in the asymptotic long-time regime but for all times, even for time-dependent diffusion constants.

We now assume that the transition rate Γ only depends on the potential depth $V_m = |V(x, y)|$ of the trapping site. Furthermore, we introduce the probability $P(V_m, t)\mathrm{d}V_m$ for a colloid to be at time t in a minimum with the depth within the interval $[V_m, V_m + \mathrm{d}V_m]$. In the following, we will study diffusion based on the rate equation for $P(V_m, t)$ instead of using $p(x, y, t)$. However, this is only possible if the transition rates Γ do not depend on the location of the trapping sites and, especially, if there are no positional correlations of the transition rates.

To calculate the diffusion constant from equation (11), all trapping sites with equal V_m are put together so that the average in space is replaced by an average over all possible depths V_m:

$$D(t) = \frac{zl^2}{4}\int_0^{V_0} \mathrm{d}V_m \Gamma(V_m)P(V_m, t). \quad (13)$$

Note that the values for the depth V_m are limited to the range 0 to V_0. The rate equation for $P(V_m, t)$ reads

$$\frac{\mathrm{d}}{\mathrm{d}t}P(V_m, t) = -z\Gamma(V_m)P(V_m, t) + z\rho(V_m)\int_0^{V_0} \mathrm{d}V_m' \Gamma(V_m')P(V_m', t). \quad (14)$$

The first term on the right-hand side is the probability of a colloid to leave a trapping site of depth V_m; the second term gives the averaged probability that the colloid jumps into the potential minimum of this site. The probability density $\rho(V_m)$, already introduced at the end of Section 2 for the decagonal potential, takes into account the distribution of potential depths. In accordance with Γ, $\rho(V_m)$ also does not depend on position. The Laplace transform of equation (14) with respect to time reads

$$s\overline{P}(V_m, s) - P_0(V_m) = -z\Gamma(V_m)\overline{P}(V_m, s) + z\rho(V_m)\int_0^{V_0} \mathrm{d}V_m' \Gamma(V_m')\overline{P}(V_m', s), \quad (15)$$

where $\overline{P}(V_m, s) = \int_0^\infty \mathrm{d}t \exp(-st)P(V_m, t)$ is the Laplace transform of $P(V_m, t)$ and $P_0(V_m) = P(V_m, t = 0)$ is the distribution at $t = 0$. To solve equation (15), we define

$$c(s) = \int_0^{V_0} \mathrm{d}V_m' \Gamma(V_m')\overline{P}(V_m', s), \quad (16)$$

and calculate $\overline{P}(V_m, s)$ from equation (15):

$$\overline{P}(V_m, s) = \frac{P_0(V_m)}{z\Gamma(V_m) + s} + \frac{z\rho(V_m)}{z\Gamma(V_m) + s}c(s). \quad (17)$$

Inserting equation (17) into (16) and solving for $c(s)$ gives

$$c(s) = \frac{\int_0^{V_0} \mathrm{d}V_m' \frac{\Gamma(V_m')P_0(V_m')}{z\Gamma(V_m')+s}}{s\int_0^{V_0} \mathrm{d}V_m' \frac{\rho(V_m')}{z\Gamma(V_m')+s}}\,. \quad (18)$$

Equation (18) together with (17) represents the Laplace transform of the solution to the rate equation (14).

We are interested in the long-time behavior of the diffusion constant (13). In the following, we show that the system relaxes exponentially to the asymptotic diffusion constant D_∞ on a time scale given by τ:

$$D(t) = D_\infty(1 + e^{-t/\tau}). \tag{19}$$

We determine the long-time behavior of $D(t)$ in equation (13) from its Laplace transform

$$\overline{D}(s) = \frac{zl^2}{4}\int_0^{V_0} \mathrm{d}V_m \Gamma(V_m)\overline{P}(V_m, s), \tag{20}$$

by investigating $\overline{D}(s)$ for small s. To linear order in s, the Laplace transform of equation (19) is $s\overline{D}(s) \approx D_\infty(1+s\tau)$. Comparing it to the expansion of $s\overline{D}(s)$ given by equations (17, 18), and (20), we can identify the asymptotic diffusion constant

$$D_\infty = \lim_{t\to\infty} D(t) = \lim_{s\to 0} s\overline{D}(s) = \frac{zl^2}{4\int_0^{V_0}\mathrm{d}V_m \frac{\rho(V_m)}{\Gamma(V_m)}} \tag{21}$$

and the time scale

$$\tau = \frac{1}{z}\frac{\int_0^{V_0}\mathrm{d}V_m \frac{\rho(V_m)}{\Gamma(V_m)^2}}{\int_0^{V_0}\mathrm{d}V_m \frac{\rho(V_m)}{\Gamma(V_m)}} + \frac{1}{z}\int_0^{V_0}\mathrm{d}V_m \frac{\rho(V_m) - P_0(V_m)}{\Gamma(V_m)}. \tag{22}$$

Note that equation (21) corresponds to the well-known result

$$D_\infty = \frac{zl^2}{4\left\langle \frac{1}{\Gamma(V_m)}\right\rangle}, \tag{23}$$

where $\langle\cdot\rangle$ means average over all trapping sites (see, *e.g.*, [24,25]). However, in addition to being able to calculate the asymptotic diffusion constant D_∞, we also determine here the time scale on which the system relaxes into the diffusive regime.

For $\beta V_m \gg 1$ the transition rate $\Gamma(V_m)$ can be approximated by Kramer's formula [48]:

$$\Gamma(V_m) = \frac{\omega_m\omega_b}{2\pi\gamma}e^{-\beta V_m}. \tag{24}$$

Here, ω_m and ω_b are the square roots of the absolute values of the curvatures taken, respectively, at the potential minimum and the maximum of the potential barrier, the particle tries to overcome. For the regular square lattice, $\omega_b = \omega_m$ and we find using equation (2):

$$\Gamma(V_m) = \frac{\pi V_m}{\gamma l^2}e^{-\beta V_m}. \tag{25}$$

In the random square lattice, the curvature or second derivative of the potential is not continuous for a maximum situated between two minima. However, it is reasonable to take the one-sided value coming from the minimum the particle is trying to leave. Then $\omega_b = \omega_m$ and equation (25) still holds.

We now use equation (25) to determine for $\beta V_0 \gg 1$ the asymptotic diffusion constant D_∞ and the time scale τ for the relaxation into the diffusive regime. The regular square potential has only one possible minimum value, *i.e.*, $\rho(V_m) = V_0\delta(V_m - V_0)$. So evaluating equations (21) and (22), we arrive at

$$D_\infty^{(reg)} = \frac{\pi z V_0}{4\gamma}e^{-\beta V_0} \tag{26}$$

and

$$\tau^{(reg)} = \frac{\gamma l^2}{\pi z V_0}e^{\beta V_0}. \tag{27}$$

Next we calculate D_∞ and τ for the random square potential. We will also use these results as an approximation for the decagonal potential. For $\beta V_0 \gg 1$, the integrals in equations (21) and (22) are determined by the behavior close to V_0 due to the exponential dependence of $\Gamma(V_m)$ on βV_m. We therefore expand $\log[\rho(V_m)/\Gamma(V_m)]$ and similar expressions for the other integrands around V_0 to linear order in $V - V_0$. Using these expansions in the various integrals of equations (21) and (22), we arrive at the approximate values

$$D_\infty^{(rand/deca)} \approx \frac{\pi z\beta V_0}{4\gamma\rho(V_0)}e^{-\beta V_0} \tag{28}$$

and

$$\tau^{(rand/deca)} \approx \frac{\gamma l^2}{2\pi z V_0}e^{\beta V_0}. \tag{29}$$

To apply equations (28) and (29) to the decagonal potential, an average number z for the nearest neighbors and an average step length l will be introduced in Section 5. Note that the approximate time scale $\tau^{(rand/deca)}$ is the largest possible time scale of the system since it is associated with the deepest potential minimum at V_0 and therefore with the smallest of all possible Kramer's escape rates in the random or the decagonal potentials. Smaller time scales associated with smaller potential depths can be neglected in the approximate value of $\tau^{(rand/deca)}$. Nevertheless, they are responsible for the fact that in random and decagonal potentials (see Figs. 4(b) and (c)) the subdiffusion regime extends over several magnitudes in time where the Brownian particle explores the potential landscape and encounters minima which become deeper and deeper. This is clearly demonstrated by the decrease of the mean-potential energy in Figures 4(e) and (f). Only when the particle finds potential minima close to the deepest possible value V_0, does it enter the normal diffusion regime. Note that this is also consistent with the fact that for potential landscapes, where the minimum value is not limited from below, the colloidal particle will always exhibit subdiffusion [12,20–23]. In the regular cubic lattice, on the contrary, only one characteristic time scale exists and, therefore, a sharp transition to conventional diffusion occurs (see Fig. 4(a)) when the particle escapes the potential minimum in which it has relaxed in the beginning. We also remark that in the approximate value of $\tau^{(rand/deca)}$ the initial distribution $P_0(V_m)$ does not appear anymore,

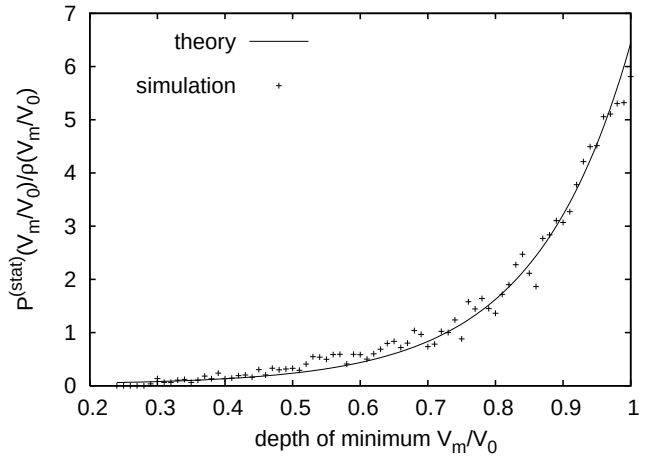

Fig. 6. Stationary distribution $P^{(stat)}(V_m)$ in the long-time limit for the decagonal potential with $\beta V_0 = 8$.

i.e., the transition to the stationary diffusion regime occurs on time scales independent of the initial conditions.

The stationary distribution $P^{(stat)}(V_m)$, which occurs in the limit of $t \to \infty$, can easily be calculated. Comparing equations (13) and (21), one finds

$$P^{(stat)}(V_m) = \frac{\frac{\rho(V_m)}{\Gamma(V_m)}}{\int_0^{V_0} \mathrm{d}V_m' \frac{\rho(V_m')}{\Gamma(V_m')}} \,. \tag{30}$$

Note that stationary distribution means $\frac{\mathrm{d}}{\mathrm{d}t} P^{(stat)}(V_m) = 0$. On the other hand, the distribution in real space $p(x, y, t)$ is not stationary for infinite systems. It is a big advantage of our approach, which is based on the distribution $P(V_m, t)$ for the depth of the trapping sites instead of the positional distribution $p(x, y, t)$, that $P(V_m, t)$ relaxes into a stationary long-time limit when the transition into the diffusive regime takes place. This is illustrated in Figures 4(a) to (c) and Figures 4(d) to (f). When the regime of normal diffusion is reached, the mean potential energy (see Figs. 4(d) to (f)) assumes a constant value in time. Finally, Figure 6 presents $P^{(stat)}(V_m)$ for the decagonal potential with $\beta V_0 = 8$ as given by the analytic formula (30) and compares it to the stationary distribution determined in the Brownian dynamics simulations in the long-time limit. As it is obvious, both theory and simulation agree very well.

5 Results of the random trap model and comparison to the simulations

The trap model developed in the last section can be used to determine the full time dependence of the mean-square displacement when the ensemble of single colloidal random walkers approaches thermal equilibrium. From a discretized version of the rate equation (14), the probability density $P(V_m, t)$ is calculated starting from $P(V_m, 0) = \varrho(V_m)$. Choosing $\varrho(V_m)$ as the initial distribution $P(V_m, 0)$, corresponds to the random initial position of the colloids used in the Brownian dynamics simulations. After $D(t)$ is calculated from equation (13), the mean-square displacement follows from integrating $D(t) = \frac{\mathrm{d}}{\mathrm{d}t}\langle r^2(t)\rangle/4$. Figures 7(a) and (b) show its dependence on time for the random square and the decagonal potential, respectively. For both potentials the graphs look similar which means that the differences in the distributions $\varrho(V_m)$, entering the rate equation (14), do not have a pronounced effect. The curves agree qualitatively with the respective simulation results in Figures 4(b) and (c). Only the short-time behavior differs substantially. This is due to the fact that in the Brownian dynamics simulations the colloids relax fastly from their random initial positions into the nearest minima whereas in the trap model the colloids are already located in these minima.

With the numerically determined probability density $P(V_m, t)$, the temporal evolution of the average depth $-\langle V_m\rangle/V_0$ of the occupied minima is readily calculated and illustrated in Figures 7(c) and (d) for the random square and the decagonal potential, respectively. The results of the Brownian dynamics simulations are nicely reproduced. In the random square potential, we find again that $-\langle V_m\rangle/V_0$ reaches its constant thermal-equilibrium value for low potential strengths βV_0 (see small arrows in Fig. 7(c)), whereas for larger values of βV_0 the steady decrease of $-\langle V_m\rangle/V_0$ is observed which for $\beta V_0 = 25$ and 50 looks nearly like a straight line exactly as for $\langle V\rangle/V_0$ in the simulations (compare Fig. 4(e)). The sharp bends in Figure 4(e) are not visible because they take place when the particles settle into a nearby minimum from a random spatial location which is not included in the random trap model, as already discussed. Similarly, in the decagonal potential (see Fig. 7(d)) a constant value for the average depth $-\langle V_m\rangle/V_0$ is reached that decreases with increasing βV_0. For further increasing βV_0, a plateau develops exactly as in the Brownian dynamics simulations. For $\beta V_0 = 50$, the average depth $-\langle V_m\rangle/V_0$ does not noticeably decrease from its starting value $-\int_0^{V_0} V_m \varrho(V_m)\mathrm{d}V_m/V_0$ at -0.603. This means most of the particles remain trapped in their initial V_m state. Since the difference in the dynamics of $P(V_m, t)$ for the random square and the decagonal potential is mainly determined by the distribution $\rho(V_m)$ for the depths of the minima, it is clear that the different temporal evolutions of $-\langle V_m\rangle/V_0$ have to be explained by the differences in $\rho(V_m)$. This we have already done in Section 3.

Our trap model in Section 4 gives analytic expressions for the asymptotic diffusion constant D_∞ and the time scale τ on which the diffusive regime is approached (see Eqs. (26, 27) for the regular square lattice and Eqs. (28, 29) for the random square and decagonal potential). So when we plot the mean-square displacement in units of $D_\infty\tau$ as a function of time in units of τ, we expect the different curves of the Brownian dynamics simulations in Figures 4(a), (b), and (c) to collapse onto a single curve in the long-time limit. This is indeed the case for the regular square potential for $\beta V_0 \gg 1$, as the main plot of Figure 8 demonstrates. Note that the trap model and especially the analytic expressions (26) to (29) are strictly valid only in the limit $\beta V_0 \gg 1$. For the random

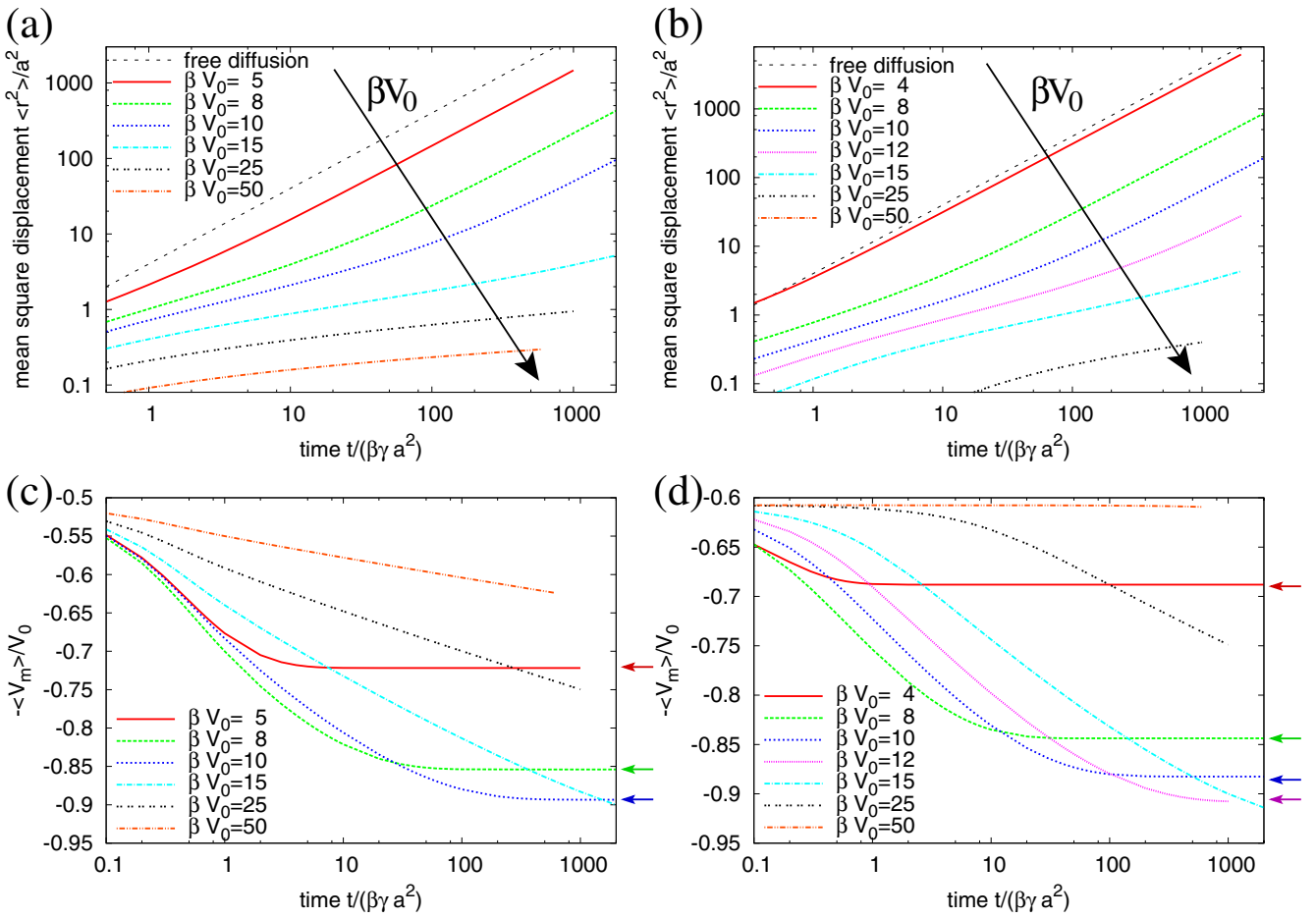

Fig. 7. Results from the random trap model: (a,b) Mean-square displacement and (c,d) average depth $-\langle V_m\rangle/V_0$ of the occupied minima as a function of time for (a,c) a random square potential and (b,d) a decagonal potential. In (a) and (b) the parameter βV_0 increases along the arrows. The small arrows on the right of (c) and (d) indicate that a stationary value for $\langle V_m\rangle/V_0$ has been reached. Lengths and times are measured, respectively, in units of a and $\beta\gamma a^2$, where a is the characteristic length scale of the potentials and γ is the particle's friction coefficient.

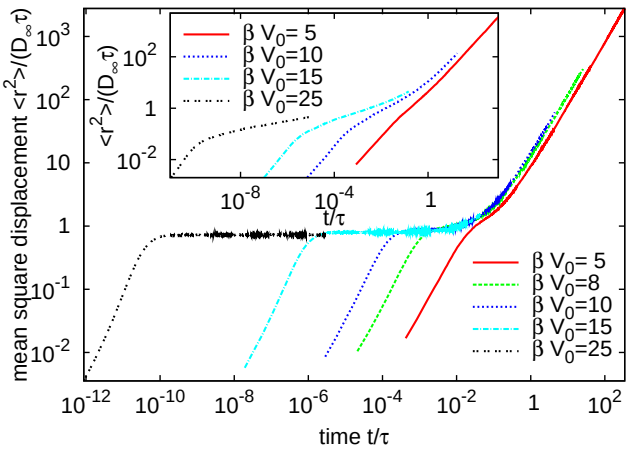

Fig. 8. Rescaled mean square displacement of the Brownian dynamics simulations in a regular square and a random square potential (inset).

square potential (see inset of Fig. 8), the rescaled curves are close together, however the collapse is not as good as in the regular case.

To calculate the asymptotic diffusion constant D_∞ and the time scale τ for the decagonal potential from equations (28) and (29), mean values for the number of nearest neighbors z and the nearest-neighbor distance l are needed, as well as the probability density $\rho(V_0)$ for potential depths close to V_0 (see Fig. 3). We obtained these values by analyzing the positions and depths of the local minima. Since the decagonal potential is not periodic, we chose a rectangular area whose edges along the x and y directions have lengths that are close to multiples of the characteristic length scales in our problem; namely $2\pi/G_{0x}$, $2\pi/G_{1x}$, $2\pi/G_{2x}$ and $2\pi/G_{1y}$, $2\pi/G_{2y}$, respectively. Periodically repeating the area, would then produce a good approximation for the quasiperiodic potential. To be concrete, we analyzed 24094 minima in an area given by $0 \le x < 110a = 110{\cdot}2\pi/G_{0x} \approx 34{\cdot}2\pi/G_{1x} \approx -89{\cdot}2\pi/G_{2x}$ and $0 \le y < 89/\sin(\frac{2\pi}{5})a = 89 \cdot 2\pi/G_{1y} \approx 55 \cdot 2\pi/G_{2y}$.

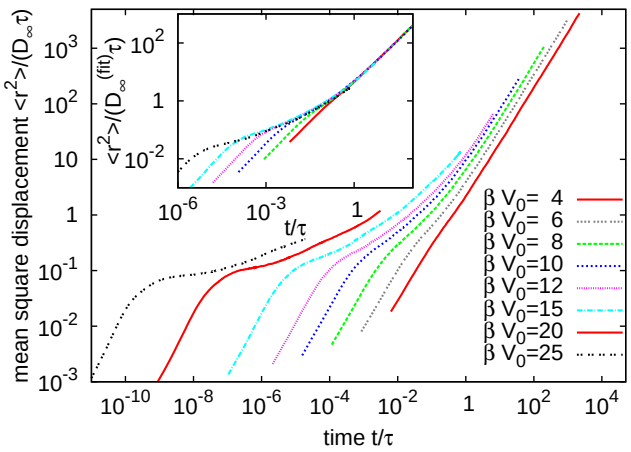

Fig. 9. Rescaled mean square displacement of the Brownian dynamics simulations in a decagonal potential. In the inset the diffusion constants from asymptotic fits are used for the rescaling.

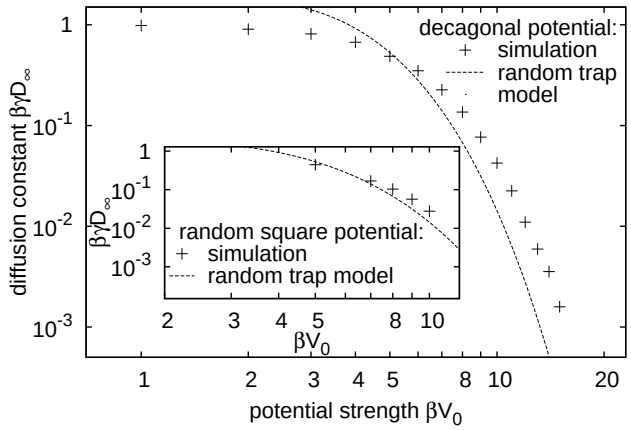

Fig. 10. Diffusion constant D_∞ in the long-time limit as a function of the potential strength βV_0 for the decagonal and the random square (inset) potential. Comparison of the random trap model and Brownian dynamics simulations.

The nearest neighbors of a potential minimum were identified with the help of a Delauney triangulation [49], which gave $z = 5.85$ and $l = 0.73a$; furthermore we found $\rho(V_0) = 0.97$.

Figure 9 presents the rescaled mean-square displacement for the decagonal potential as determined from the Brownian dynamics simulations. As in the random square potential in the inset of Figure 8, the rescaled curves are close to each other but do not exactly collapse onto a single curve. In the inset of Figure 9 we therefore used asymptotic diffusion constants $D_\infty^{(\mathrm{fit})}$ for the rescaling, which are obtained by fitting the curves from the simulations, whereas for τ still the analytic values are used. Now the rescaled curves collapse very well onto a single curve in the long-time limit indicating that the analytic approximation for τ fits very well to the simulations. On the other hand, there are differences between the numerically determined asymptotic diffusion constants $D_\infty^{(\mathrm{fit})}$ and the analytic values D_∞, as Figure 10 demonstrates. Here we plot them as a function of the potential strength βV_0. The differences might be explained by the observation that our random trap model is only approximately valid. There are always very shallow minima in the potential landscape where the particle is not bound to the minima and during the "jump" between two minima finite-time excursions outside the minima occur. Furthermore, jumps exist that do not take place between nearest neighbors, which we defined through the Delaunay triangulation, and spatial correlations in the depths of the potential wells are also completely neglected in our model. As the inset of Figure 10 demonstrates, trap model and simulations agree better for the random square potential.

6 Conclusions

Quasicrystalline systems are very appealing but also counterintuitive since they exhibit long-range positional order without having a single unit cell which is just repeated in space as in conventional crystals. In this article, we explore the Brownian motion of an ensemble of single particles in a quasicrystalline potential landcape and compare it to the motion in a regular square and a random square potential. While Brownian motion is naturally treated in equilibrium, we let the ensemble of single Brownian particles start from a non-equilibrium distribution and monitor how they reach thermal equilibrium. Brownian dynamics simulations clearly show that after a fast relaxation in local potential minima, the particles in the random square and regular potential pass a wide-stretched subdiffusive regime and then enter thermal equilibrium with respect to their energy exactly when they start to exhibit normal diffusive motion. Whereas the mean-square displacement as a function of time looks qualitatively the same for both potentials, the temporal evolution of the mean potential energy reveals differences which we explain by the different distributions for the depths of the potential minima.

We, furthermore, develop a random trap model based on the probability distribution $P(V_m, t)$ of finding a particle in a trap with depth V_m. It agrees with the results from the Brownian dynamics simulations, especially the temporal evolution of the average potential energy with its characteristic features is reproduced. While an analytic formula only approximates the long-time diffusion constant, found in the Brownian dynamics simulations, the analytically given time scale on which the particle relaxes into the diffusive state fits very well to the simulations. Finally, our model clearly identifies that normal diffusion is reached when $P(V_m, t)$ approaches its stationary distribution that corresponds to thermal equilibrium. While conventional treatments of Brownian motion use a positional distribution $p(x, y, t)$, our work here introduces an alternative approach that is easier to treat and that might be applicable to other systems where Brownian motion in an external potential is studied.

Although the quasicrystalline potential exhibits long-range positional order, we demonstrate in this article that

the non-equilibrium Brownian motion is very similar to the motion in a random potential. Especially, we find a widely stretched subdiffusive regime which is due to the wide distribution of depths of potential minima. Our article, therefore, contributes to exploring the properties of quasicrystalline structures but also to the study of systems far from equilibrium.

We would like to thank J. Baumgartl, C. Bechinger, A. Fingerle, T. Franosch, E. Frey, S. Herminghaus, G. Maret, M.F. Miri, N. Rivier, and V. Zaburdaev for helpful discussions. We also acknowledge financial support from the Deutsche Forschungsgemeinschaft under Grant No. Sta 352/5-2 and Ro 924/5-1, and the International Graduate College at the University of Konstanz.

References

1. A. Einstein, Ann. Phys. (Leipzig) **17**, 549 (1905).
2. E. Frey, K. Kroy, Ann. Phys. (Leipzig) **14**, 20 (2005).
3. A.V. Indrani, S. Ramaswamy, Phys. Rev. Lett. **73**, 360 (1994).
4. F.H. Stillinger, Science **267**, 1935 (1995).
5. C.A. Angell, Science **267**, 1924 (1995); M.D. Ediger, C.A. Angell, S.R. Nagel, J. Phys. Chem. **100**, 13200 (1996).
6. E.R. Weeks, J.C. Crocker, A.C. Levitt, A. Schofield, D.A. Weitz, Science **287**, 627 (2000); E.R. Weeks, D.A. Weitz, Chem. Phys. **284**, 361 (2002); Phys. Rev. Lett. **89**, 095704 (2002).
7. D.G. Levitt, Phys. Rev. A **8**, 3053 (1973).
8. Q.-H. Wei, C. Bechinger, P. Leiderer, Science **287**, 625 (2000).
9. C. Lutz, M. Kollmann, C. Bechinger, Phys. Rev. Lett. **93**, 026001 (2004).
10. M. Kollmann, Phys. Rev. Lett. **90**, 180602 (2003).
11. F. Höfling, T. Franosch, E. Frey, Phys. Rev. Lett. **96**, 165901 (2006).
12. Y. Kafri, D.K. Lubensky, D.R. Nelson, Biophys. J. **86**, 3373 (2004).
13. M. Weiss, M. Elsner, F. Kartberg, T. Nilsson, Biophys. J. **87**, 3518 (2004).
14. F. Amblard, Phys. Rev. Lett. **77**, 4470 (1996).
15. P. Bursac, G. Lenormand, B. Fabry, M. Oliver, D.A. Weitz, V. Viasnoff, J.P. Butler, J.J. Fredberg, Nat. Mater. **4**, 557 (2005).
16. P. Smith, I.E.G. Morrison, K.M. Wilson, N. Fernandez, R.J. Cherry, Biophys. J. **76**, 3331 (1999).
17. P. Schwille, U. Haupts, S. Maiti, W.W. Webb, Biophys. J. **77**, 2251 (1999).
18. I. Golding, E.C. Cox, Phys. Rev. Lett. **96**, 098102 (2006).
19. T.J. Feder, I. Brust-Mascher, J.P. Slattery, B. Baird, W.W. Webb, Biophys. J. **70**, 2767 (1996).
20. J. Honkonen, Y.M. Pis'mak, J. Phys. A **22**, L899 (1989).
21. A.H. Romero, J.M. Sancho, Phys. Rev. E **58**, 2833 (1998).
22. J.M. Sancho, A.M. Lacasta, K. Lindenberg, I.M. Sokolov, A.H. Romero, Phys. Rev. Lett. **92**, 250601 (2004).
23. A.M. Lacasta, J.M. Sancho, A.H. Romero, I.M. Sokolov, K. Lindenberg, Phys. Rev. E **70**, 051104 (2004).
24. J.W. Haus, K.W. Kehr, J.W. Lyklema, Phys. Rev. B **25**, 2905 (1982).
25. J.W. Haus, K.W. Kehr, Phys. Rep. **150**, 263 (1987).
26. Derrida, J. Stat. Phys. **31**, 433 (1983).
27. D. Shechtman, I. Blech, D. Gratias, J.W. Cahn, Phys. Rev. Lett. **53**, 1951 (1984).
28. D.A. Rabson, N.D. Mermin, D.S. Rokhsar, D.C. Wright, Rev. Mod. Phys. **63**, 699 (1991).
29. B. Passaro, C. Sire, V.G. Benza, Phys. Rev. B **46**, 13751 (1992).
30. L. Guidoni, B. Dépret, A. di Stefano, P. Verkerk, Phys. Rev. A **60**, R4233 (1999).
31. R. McGrath, J. Ledieu, E.J. Cox, R.D. Diehl, J. Phys.: Condens. Matter **14**, R119 (2002).
32. M. Shimoda, T.J. Sato, A.P. Tsai, J.Q. Guo, Phys. Rev. B **62**, 11288 (2000).
33. K.J. Franke, H.R. Sharma, W. Theis, P. Gille, Ph. Ebert, K.H. Rieder, Phys. Rev. Lett. **89**, 156104 (2002).
34. V. Fournée, T.C. Cai, A.R. Ross, T.A. Lograsso, J.W. Evans, P.A. Thiel, Phys. Rev. B **67**, 033406 (2003).
35. J. Ledieu, J.T. Hoeft, D.E. Reid, J.A. Smerdon, R.D. Diehl, T.A. Lograsso, A.R. Ross, R. McGrath, Phys. Rev. Lett. **92**, 135507 (2004).
36. R.A. Tasca, N. Ferralis, R.D. Diehl M.W. Cole, J. Phys.: Condens. Matter **16**, S2911 (2004).
37. S. Curtarolo, W. Setyawan, N. Ferralis, R.D. Diehl, M.W. Cole, Phys. Rev. Lett. **95**, 136104 (2005).
38. A. Ashkin, Phys. Rev. Lett. **24**, 156 (1970); Science **210**, 1081 (1980).
39. M.M. Burns, J.M. Fournier, J.A. Golovchenko, Science **249**, 749 (1990).
40. A. Chowdhury, B.J. Ackerson, N.A. Clark, Phys. Rev. Lett. **55**, 833 (1985).
41. Q.-H. Wei, C. Bechinger, D. Rudhardt, P. Leiderer, Phys. Rev. Lett. **81**, 2606 (1998); C. Bechinger, M. Brunner, P. Leiderer, Phys. Rev. Lett. **86**, 930 (2001); M. Brunner, C. Bechinger, Phys. Rev. Lett. **88**, 248302 (2002); J. Baumgartl, M. Brunner, C. Bechinger, Phys. Rev. Lett. **93**, 168301 (2004).
42. J. Chakrabarti, H.R. Krishnamurthy, A.K. Sood, Phys. Rev. Lett. **73**, 2923 (1994); J. Chakrabarti, H.R. Krishnamurthy, A.K. Sood, S. Sengupta, Phys. Rev. Lett. **75**, 2232 (1995).
43. M. Schmiedeberg, J. Roth, H. Stark, Phys. Rev. Lett. **97**, 158304 (2006).
44. For example it takes approximatly 90 s CPU time per million steps per particle on one unit of an AMD Athlon64 X2 Dual-Core 4600+ (2.4 GHz) processor.
45. S.P. Gorkhali, J. Qi, G.P. Crawford, J. Opt. Soc. Am. B **23**, 149 (2005).
46. A.A. Chernikov, R.Z. Sagdeev, D.A. Usikov, G.M. Zaslavsky, Phys. Lett. A **125**, 101 (1987).
47. D. Levine, T.C. Lubensky, S. Ostlund, S. Ramaswamym, P.J. Steinhardt, J. Toner, Phys. Rev. Lett. **54**, 1520 (1985); J.E.S. Socolar, T.C. Lubensky, P.J. Steinhardt, Phys. Rev. B **34**, 3345 (1986).
48. P. Hänggi, P. Talkner, M. Borkovec, Rev. Mod. Phys. **62**, 251 (1990).
49. R. Collins, J. Phys. C **1**, 1461 (1968); J.L. Meijering, Philips Res. Rep. **8**, 270 (1953).